Interaction Between SH_0 Guided Waves and Tilted Surface-Breaking Cracks in Plates

Jérôme Combaniere, Peter Cawley, Kevin McAughey, and Jochen Giese

***Abstract*— The interaction between SH_0 guided waves and simple defects is well understood and documented, and the SH_0 and related torsional guided waves are commonly used in inspection. However, tilted and branching cracks, for which vertical notches are a poor approximation, are found in some environments, particularly when pipes are buried in alkaline soils. This paper studies the interaction between SH_0 guided waves and tilted, surface-breaking cracks, investigating the effect of the tilt and depth of the defect. The incident wave interacts with the tilted crack to generate a transmitted wave, a reflected wave, and a wave trapped below the crack. It is shown that the direction of the tilt of the crack relative to the incident wave direction does not affect the scattering behavior. In addition, the axial extent of the crack plays a major role in the reflectivity of the crack, leading to transmission nulls in some configurations. These transmission nulls appear for all crack depths, the frequency range over which the transmission is significantly reduced increasing with crack depth. This behavior is shown to be analogous to the acoustic energy flow in a duct when a Helmholtz resonator is introduced. The null is not seen above the SH_1 cutoff as the propagating signals are no longer monomodal. The existence of a transmission null and corresponding reflection maximum is promising for the detection of small defects and measurement of the frequency at which the null occurs will assist with defect characterization. Experimental validations of the key results are presented.**

***Index Terms*— Crack, guided waves, resonator, tilt.**

I. Introduction

With over 1 500 000 km of pipelines around the world carrying oil, gas, or petroleum [1], monitoring their state and assessing their remaining life are a major concern. Since more than 90% of in-use pipelines are buried underground or are underwater, one commonly used method to monitor their physical integrity is through the use of inspection pigs [2]. Pigs can use either magnetic or ultrasonic inspection, with both bulk and guided ultrasonic waves being employed in the latter case. To detect axially aligned cracks, pigging tools can use circumferential guided waves from either both the Rayleigh–Lamb or shear horizontal (SH) families [3]. The interaction of guided waves with vertical cracks, notches, and delaminations has been intensively studied over many years, both analytically and using finite-element simulations. These simple defect geometries are good approximations for a majority of commonly found defects. However, tilted and branching cracks, for which vertical notches are not a good approximation, are found in some environments, particularly when pipes are buried in alkaline soils [4]–[8]. The interaction between guided waves and these more complex defects needs to be addressed.

Recently, Guan *et al.* [9] reviewed the general use of guided waves for damage identification in pipeline structures. Of specific relevance to the phenomena discussed in this paper, Alleyne and Cawley [10] investigated the relationship between the reflection of simple zero order Lamb waves and the frequency-thickness product at which the inspection is carried out, noting the presence of minima in the transmission ratio at particular frequency-thickness products. Chennamsetti [11] studied the interaction between the fundamental Lamb modes and the front edge of a noncentrally aligned delamination in a metallic plate, showing that the incident wave undergoes transmission, reflection, and mode conversion when reaching the front end of the delamination. The transmitted waves propagate in both subwaveguides, above and below the delamination. Mode-converted Lamb modes also propagate in all three parts (main waveguide for the reflected, mode converted wave, and both subwaveguides for the transmitted, mode converted waves) of the plate. More recently, Schaal and Mal [12] worked with Lamb waves propagating in plates with step discontinuities and showed that, in the near field of the step discontinuity, evanescent modes are physically present in both propagating directions, together forming standing waves that do not transport energy.

This paper considers the interaction of SH waves with tilted defects. Again, there have been numerous studies on their interaction with vertical cracks and notches. Regarding the simpler case of SH waves below the SH_1 cutoff frequency interacting with defects, Demma *et al.* [13] studied the reflection behavior of the fundamental SH_0 mode from rectangular notches, investigating the effect of the axial extent of the defect, its depth, and the frequency-thickness product. They observed reflection nulls caused by destructive interference

Manuscript received July 18, 2018; accepted October 15, 2018. Date of publication October 18, 2018; date of current version January 14, 2019. This work was supported in part by the U.K. Engineering and Physical Sciences Research Council and U.K. Research Center in Non-Destructive Evaluation through an Engineering Doctorate studentship for J. Combaniere under Grant EP/L015587/1 and in part by Baker Hughes, a GE company. *(Corresponding author: Jérôme Combaniere.)*

J. Combaniere is with the Department of Mechanical Engineering, Imperial College London, London SW7 2AZ, U.K., and also with Baker Hughes, a GE company, Cramlington NE23 1WW, U.K. (e-mail: j.combaniere16@imperial.ac.uk).

P. Cawley is with the Department of Mechanical Engineering, Imperial College London, London SW7 2AZ, U.K.

K. McAughey is with Baker Hughes, a GE company, Cramlington NE23 1WW, U.K.

J. Giese was with Baker Hughes, a GE company, 76297 Blankenloch-Stutensee, Germany.

Digital Object Identifier 10.1109/TUFFC.2018.2876723

This work is licensed under a Creative Commons Attribution 3.0 License. For more information, see http://creativecommons.org/licenses/by/3.0/

between the reflected wave from one end of the notch and the reflected wave from the other end of the notch. Later, Carandente *et al.* [14] worked with several varying depth profiles such as steps, tapered notches, and V-notches, looking at the reflection modulus from such defects using the fundamental torsional mode, the equivalent of the SH_0 mode in a pipe structure. Recently, Lee *et al.* [15] have used a closed form solution based on the reciprocity theorem to obtain similar results to those found using finite-element analysis in [13], [14].

Three decades ago, Koshiba *et al.* [16] derived a solution for the scattering of SH waves in an elastic plate using a combination of the finite-element method to investigate the propagation of the waves in the region of the defect and an analytical method to model their propagation in the waveguides surrounding the discontinuity. They took into account both the propagating and evanescent higher order modes to determine the scattering obtained from a step discontinuity, a wedge-shaped crack, and a strip of another material rigidly coupled to the surface of the plate. Ditri [17] studied the scattering of SH waves from step discontinuities in the material properties and/or geometry of otherwise uniform flat layer waveguides; he also proposed and proved a noncoupling condition which explains why particular modes are not generated in the scattering process. More recently, Pau *et al.* [18] used a novel method based on the principle of reciprocity in elastodynamics to investigate the interaction of the SH_0 mode with discontinuities in plate waveguides. They highlighted the different regimes that arise from the interaction between the SH_0 mode and a discontinuity, either symmetric or nonsymmetric, consisting of sharp changes in thickness. In the case of frequency-thickness products above the cutoff of higher order modes, they observed that for both large and small changes of thickness, the mode conversion of propagating modes is small, whereas for midvalues of thickness change, mode conversion is significant. For frequency-thickness products below the SH_1 cutoff, only one regime is present since no mode conversion can occur.

With all guided wave modes, the reflection, transmission, scattering, and trapping of energy at a defect is strongly related to the defect geometry. Linton *et al.* [19] considered the existence of trapped modes near sound-hard defects in 2-D waveguides for cases where there is no symmetry about the centreline of the guide. They examined both Dirichlet and Neumann condition problems and noted that these modes exist for discrete pairs of parameters which define the geometry of the obstacle. Around the same time, Porter [20] showed that trapped waves exist for circular cutouts with free edges, of all radii, centrally placed within a waveguide with free boundary conditions placed upon the lateral boundaries. Glushkov *et al.* [21]–[25] worked extensively on trapped modes over the last decade, mainly with Lamb and Rayleigh waves in plates. They investigated delaminations, notches, and ribbed plates and showed that trapped modes could lead to a concentration of the energy localization, which they referred to as a vortex of energy. These vortices of energy would then block energy transmission and lead to band gaps in either reflection or transmission.

Two different mechanisms can lead to band gaps: destructive interference between the incoming wave and the diffracted wave and resonant capturing of the energy when the frequency used for inspection is close to a pole of the problem in the spectral domain [23]. Rokhlin [26] solved the problem of Lamb wave diffraction from a symmetrically located finite horizontal crack by the method of multiple diffractions. He showed that this diffraction is accompanied by strong resonance phenomena in the region of the crack that acts as a high-Q resonator for the waves with a high coefficient of reflection from the edges of the crack, leading to a sharp peak in the reflection coefficient for specific values of crack length. Glushkov [21], [23], [24] and Feng and Lin [27] worked on the propagation of Lamb waves in periodic ribbed plates at frequency thicknesses up to 2 MHz $\cdot$ mm. They identified several configurations for which a zero in transmission was observed, attributing it to the coupled vibrations of Lamb modes in different sliced sections of a unit cell from the periodic ribbed plate. Vinh *et al.* [28] investigated the reflectivity of the SH_0 mode at very rough interfaces; when modeling them as a periodic comblike structure, they noted that, provided a specific ratio between the periodicity of the comblike interface and the wavelength is used for inspection, a band gap appeared when looking at the transmitted signal.

This paper looks specifically at the problem of the interaction of the SH_0 mode with tilted cracks that to the best of the authors knowledge has not been previously studied, the motivation being to improve the detection and characterization of such defects during pigging operations. In Section II, the model used for simulation is presented. The main findings of this paper are developed in Section III where the effects of the sign of the tilt and the depth of the crack are investigated and nulls in transmission are highlighted for some configurations. Experimental validation of a selection of the predictions is presented in Section IV, followed by a summary of the conclusions in Section V.

II. Model Description

Although analytical approaches have been successfully applied to determine the reflectivity of simple thickness steps in plates [17] and V-notches in pipes [15], a finite-element modeling approach was used in this paper because it can be used for both the single tilt angle geometry studied here and future work on branched cracks. Unless stated otherwise, the results presented in this paper were obtained through simulations where the mesh was calculated with ABAQUS [29] and solved using the Pogo finite-element software [30]. A steel plate of constant thickness (10 mm, z-axis) and length (1850 mm, y-axis) was modeled with a surface-breaking tilted crack. For SH wave modeling, the best choice of element would be 2-D plane strain elements allowing nodal displacement in the out of plane dimension. However, such elements are not available in ABAQUS or in POGO; hence, the need to use 3-D elements that meet the required conditions and apply appropriate boundary conditions. Efficient modeling of the SH0 wave is in turn achieved by using a single-element wide layer (x-axis), with antisymmetry boundary conditions applied on the two surfaces. This condition is applied by fixing

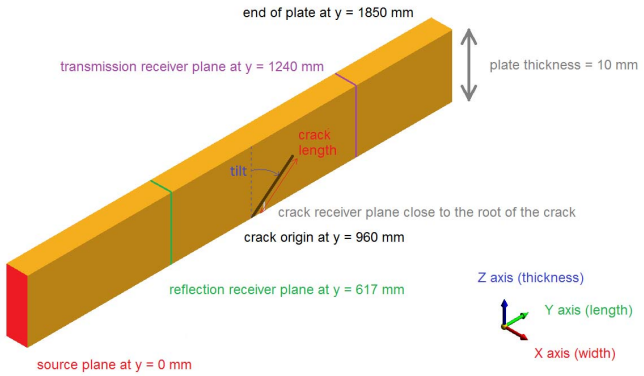

Fig. 1. Model geometry. Example for a tilt of +60° and a depth of 50% of wall thickness (not to scale).

TABLE I
PARAMETERS DESCRIBING THE FE MODEL

Parameter	Value	Unit
Steel properties		
Poisson's ratio	0.2948	-
Density	7800	$kg \cdot m^{-3}$
Young's modulus	209.75	GPa
Locations of interest on the y axis		
Excitation plane	0	mm
Reflection receiver plane	617	mm
Crack root	960	mm
Transmission receiver plane	1240	mm
End of plate	1850	mm
Input signal		
Number of cycles	5	-
Frequency	100	kHz
Windowing	Hanning	-

the nodal displacements to zero in the two surface directions (y- and z-directions), only allowing motion out of the surface (x-direction). The crack was modeled by duplicating and disconnecting the nodes across the crack face so it effectively had zero width. Since the elements on each side of the crack are disconnected and thus cannot communicate with each other, the crack is similar to a frictionless interface; this is effectively a free boundary interface. Fig. 1 represents the model for a tilt of +60° and a depth of 50% of wall thickness. The tilt represents the angle between the crack and the normal to the plate; it can be either positive, as shown in Fig. 1, when the crack is oriented in the direction of propagation of the incident wave, or negative when the crack is oriented toward the excitation plane. The relevant parameters to describe the model are shown in Table I. The plate was modeled using a free mesh with six-noded triangular prism elements (C3D6 [29]). The incident wave was generated by applying in the x-direction; the force described by the input signal in Table I on all the nodes of the source plane presented in Fig. 1 simultaneously, so preferentially exciting SH0 due to uniform motion. The shear displacement (x-direction) was monitored in two planes, as shown in Table I and Fig. 1. The

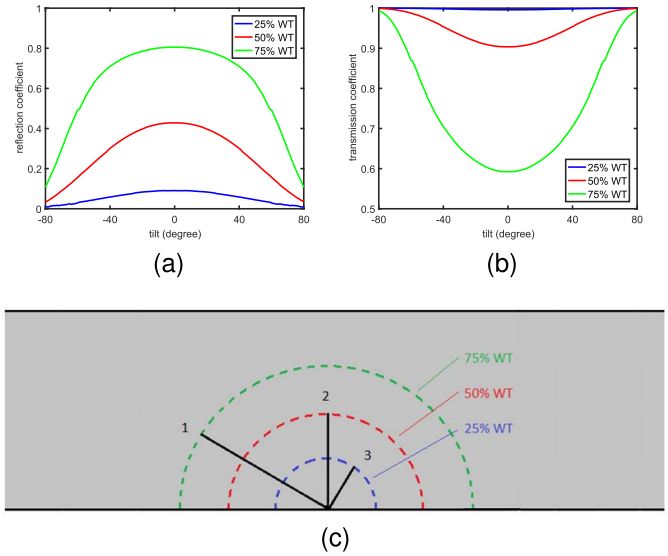

Fig. 2. Evolution of both (a) reflection coefficient and (b) transmission coefficient in a 10-mm-thick plate at 100 kHz as a function of tilt for total crack lengths of 25 wt% (blue line), 50 wt% (red line), and 75 wt% (green line) with (c) examples of tilted cracks.

mean was then computed for each plane, effectively enhancing symmetric modes and removing antisymmetric modes, since the monitored nodes were equally spaced through the thickness. All these parameters were constant throughout the simulations; the two parameters that were varied being the tilt of the crack and its depth. The model presented here was first validated by reproducing the results for vertical cracks and rectangular notches from Demma *et al.* [13].

III. INFLUENCE OF TILT ON REFLECTIVITY AND TRANSMISSIBILITY

In this section, both reflectivity and transmissibility calculations are amplitude based, as opposed to energy based, and performed in the frequency domain. Unless stated otherwise, both the reflection and the transmission coefficients are taken at the central frequency $f = 100$ kHz.

A. Comparison Between Positive and Negative Tilt

The influence of tilt angle for cracks of constant overall length but varying tilt angle (and hence varying depth through the plate thickness) was studied using cracks of overall length 25%, 50%, and 75% of the wall thickness. Fig. 2(a) shows the reflection coefficient as a function of tilt angle, while Fig. 2(b) displays the transmission coefficient in the same way, examples of the cracks being shown in Fig. 2(c). The sum of the transmission and reflection coefficients is greater than unity because they are based on amplitude, rather than energy. As part of the validation process, it was verified that the sum of the squares of the coefficients sum to unity to within 0.05%, where the discrepancy can be ascribed to numerical errors. As expected, longer cracks are more reflective than shorter cracks at all angles and it is striking that the curves are symmetric about zero tilt, showing that these coefficients are

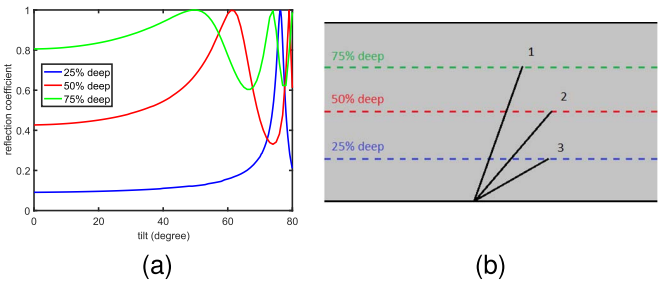

Fig. 3. Evolution of (a) reflection coefficient for different depths of crack in a 10-mm-thick plate at 100 kHz as a function of tilt with (b) examples of tilted cracks.

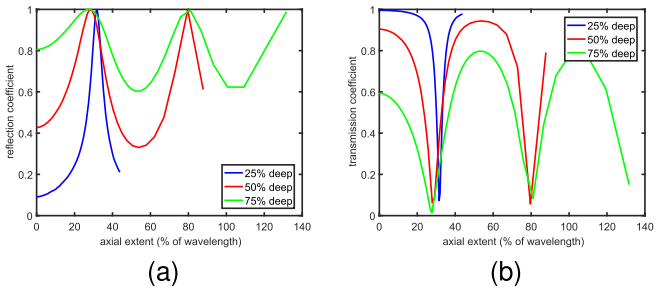

Fig. 4. Variation of (a) reflection coefficient and (b) transmission coefficient with axial extent of crack for different depths of tilted crack at 1 MHz·mm.

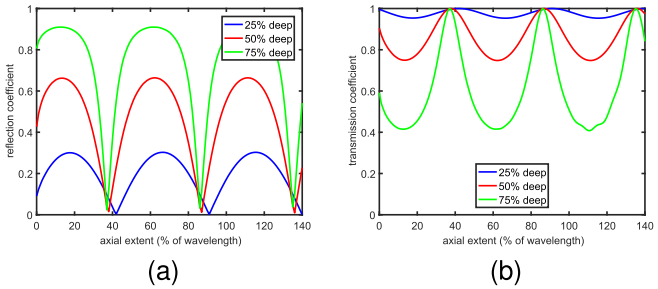

Fig. 5. Variation of (a) reflection coefficient and (b) transmission coefficient with axial extent of notch for different depths of vertical notch at 1 MHz·mm.

independent of the sign of the tilt angle. It would be expected from reciprocity that the transmission coefficient would be symmetric, and given that there is no mode conversion below the SH_1 cutoff frequency, the energy conservation requirement for the squares of the reflection and transmission coefficients to sum to unity implies that the reflection coefficient curves must also be symmetric. The maximum difference between positive and negative tilts was 1.5% and this reduced to 0.1% at angles below 60°; these differences can be ascribed to numerical errors. The increased difference in measured coefficients for highly tilted defects comes from the difficulty in modeling the root of the crack, where the elements can be very distorted. The fact that the transmission coefficient is close to unity for shallow defects [blue line in Fig. 2 (b)] is of particular importance in the field of long range guided wave inspection, since it implies small transmission loss past small features, resulting in inspection ranges of up to 100 m [31].

B. Effect of Defect Depth

The influence of tilt for cracks of constant depth was investigated for three different depths: 25%, 50%, and 75% of the wall thickness. The constant depth and varying tilt angle lead to an increase in overall crack length as the tilt increases. Fig. 3(a) shows the reflection coefficient as the tilt varies, examples of the cracks being displayed on Fig. 3(b). As expected, for the vertical (0°) case, deeper cracks generate a higher reflection. Fig. 3(a) shows that, at all depths, there are maxima and minima in the reflection coefficient; the values of the tilt for which these extrema occur depend on the depth of the crack.

Fig. 4(a) displays the same data as Fig. 3 after converting the tilt angle into the axial extent of the crack as a fraction of wavelength, while Fig. 4(b) shows the variation of the transmission coefficient with the axial extent of the crack. It is interesting to note that extrema in both reflectivity and transmissibility are now located around the same axial extent. Shallower cracks have sharper peaks, but it appears that all peaks in reflectivity approach unity reflection coefficient, implying zero transmission, as shown in Fig. 4(b). In some cases, where the troughs are very sharp, they do not quite reach zero; this is probably due to the finite step size used. For the same angle, a deeper defect has a longer axial extent than a shallower one; hence the green curve, showing results from a 75% deep crack, extends further along the axial extent axis than the others, while the maximum axial extent on the blue curve, showing the results for a 25% crack, only extends to about 40% of the wavelength. Minima in reflection can also be observed in Fig. 4(a), for cracks whose axial extent is around 55%, even though they do not reach zero. The same effect can be seen in Fig. 4(b) with maxima in transmission not reaching unity at the same values of axial extent. Similar behavior can be observed in the case of vertical notches; results from Demma *et al.* [13] were reproduced at the same depths as in the case of tilted cracks, the corresponding reflection and transmission coefficients being shown in Fig. 5(a) and (b), respectively. These show striking similarities to Fig. 4, clear maxima and minima being seen at specific values of axial extent as a proportion of the wavelength. The main difference lies in the fact that the nulls are in reflection for the notch case and in transmission for the tilted crack case. Correspondingly, perfect transmission is obtained at certain axial extents in the notch case, while total reflection is obtained at certain axial extents for tilted cracks. In both cases, the locations of these extrema are only a weak function of the feature depth.

C. Visualization of Wave Propagation and Zero Transmission Case

It is interesting that a transmission null appears to be obtained at all values of tilted crack depth, albeit the null becoming increasingly sharp as the depth reduces, and hence more difficult to observe when a relatively broadband signal is input, so giving a wider range of wavelengths. In order to understand the phenomenon better, screenshots of the motion were taken in cases close to and away from a transmission null. It must be noted that the different screenshots were not

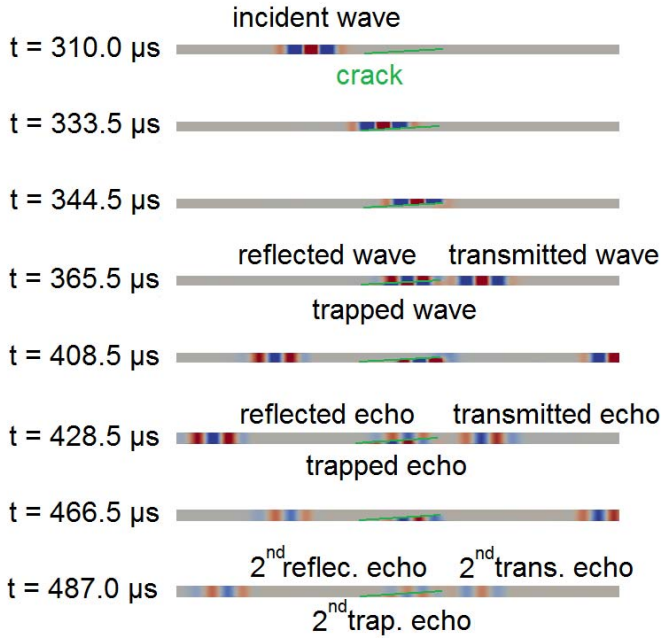

Fig. 6. Screenshots of the amplitude of the horizontal (x-direction in Fig. 7) displacement as an incident SH_0 wave with an input 2.5-cycle toneburst at a central frequency $f = 100.0$ kHz interacts with a 50% depth crack (in green) with a tilt angle of 87° in a 10-mm plate (not to scale).

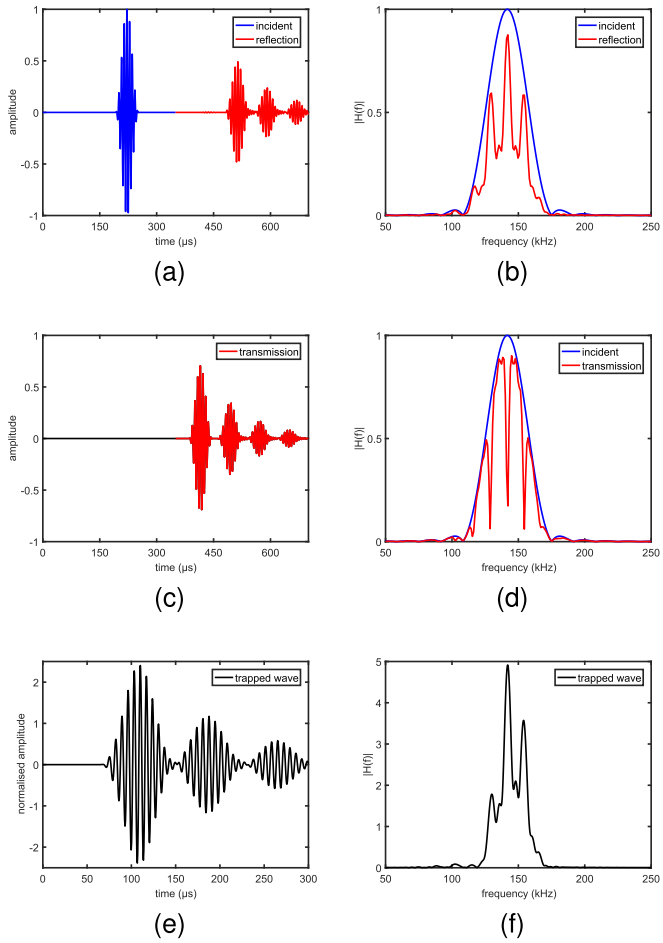

Fig. 7. Normalized reflection and transmission A-scans in the case of a 50% deep crack tilted at 87.6° in a 10-mm-thick plate with an input nine-cycle toneburst at a central frequency $f = 141.7$ kHz. (a) A-scan of the incident and reflected signals. (b) Fast Fourier transform (FFT) of the incident and reflected signals. (c) A-scan of the transmitted signal. (d) FFT of the incident and transmitted signals. (e) A-scan of the trapped signal. (f) FFT of the trapped signal.

taken at specific intervals, but rather at times where interesting phenomena were observed.

In Fig. 6, screenshots of the horizontal (x-direction of Fig. 1) displacement are taken in a case away from the transmission null, for a 50% deep crack tilted at 87° with a 2.5-cycle Hanning-windowed input signal at $f = 100.0$ kHz, the reduced number of cycles allowing a better separation, and hence identification, of the different waves. The blue color corresponds to displacements in the negative x-direction, while the red color shows positive displacements. At $t = 333.5$ μs, it can be seen that the interaction of the incident wave with the root of the crack generates a negligible reflected wave (below 0.7% of the amplitude). When the incident wave reaches the tip of the crack at $t = 344.5$ μs, it is divided into three components: a reflected wave, propagating back above the crack, a transmitted wave, propagating through the rest of the plate, and a trapped wave, propagating backwards below the crack, all three of which can be seen propagating at $t = 365.5$ μs. Since the defect is a surface-breaking crack, the trapped wave is totally reflected at the root of the defect. When the trapped wave reaches the open end of the crack at $t = 408.5$ μs, it is again partially transmitted and reflected and the process is repeated, leading to gradually decaying reverberations, examples of which can be observed in Fig. 7(a) and (b). This can also be seen when comparing the displacements at $t = 365.5$ μs, $t = 428.5$ μs, and $t = 487.0$ μs in Fig. 6, times at which different transmitted waves are located in the same area of the plate, allowing for easy comparison.

In order to understand the relative phases of the different reverberations, a narrower band signal was used. The center frequency was increased to 141.7 kHz to reduce the wave packet length and ensure that the wave packets remained separated. The normalized A-scans recorded at the reflection and transmission receiver planes (see Fig. 1) in the case of a crack tilted at 87.6° with an effective depth of 50% of the wall thickness with an input nine-cycle toneburst at a central frequency $f = 141.7$ kHz are shown in Fig. 7(a) and (b), with their respective spectra being plotted in Fig. 7(c) and (d). Both the reflection and transmission A-scans show reverberating signals resulting from the crack that, in this very oblique and hence long case, are separated in time. These result in multiple maxima and minima in the corresponding spectra. Similarly, Fig. 7(e) shows the predicted signal at a location on the surface of the plate beneath the crack, 23.8 mm (1.05 wavelength) from its root, the corresponding spectrum being shown in Fig. 7(f). The larger amplitude is caused by the reduction of the effective plate thickness at the location where the results were recorded. The minima in transmission are located at $f = 115.4$, 128.7, 142.1, and 154.5 kHz, corresponding to an axial extent of the crack of, respectively, 426.2%, 475.3%,

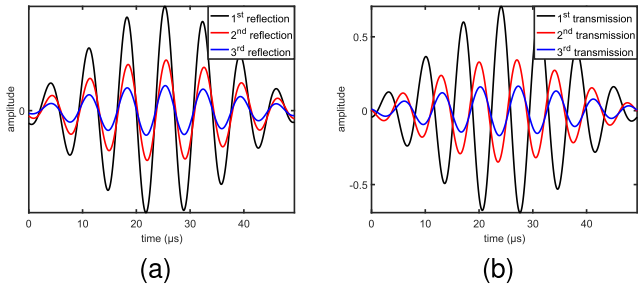

Fig. 8. Reflected (a) and transmitted (b) wave packets from Fig. 7, each centered on the maximum of their Hilbert transform.

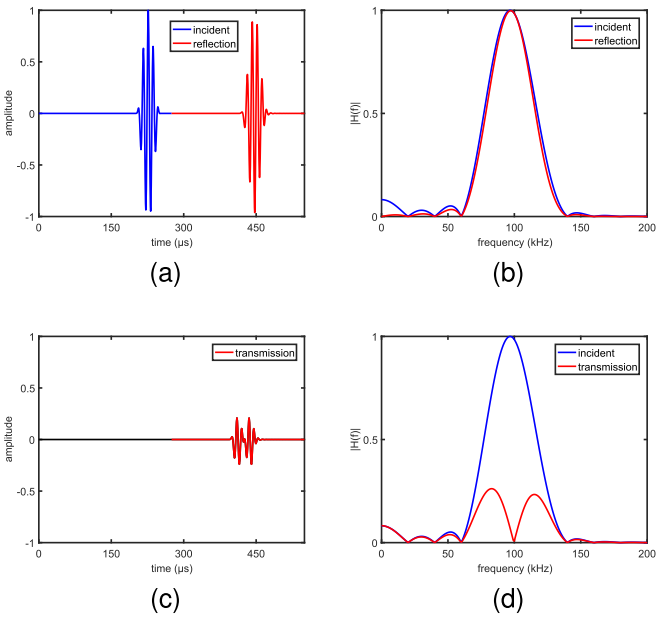

Fig. 9. Normalized reflection and transmission A-scans in the case of a 75% deep crack tilted at 50° in a 10-mm-thick plate at 100 kHz. (a) A-scan of the incident and reflected signals. (b) FFT of the incident and reflected signals. (c) A-scan of the transmitted signal. (d) FFT of the incident and transmitted signals.

524.8%, and 570.7% of the wavelength. The location of these minima is periodic, with a period of ∼50% of the wavelength and the location of the minima correspond with the locations of the maxima in the trapped wave signal of Fig. 7(f) and the reflection signal of Fig. 7(b). The phases of the different reflected and transmitted wave packets relative to that of the incident wave were investigated by gating the different wave packets and centring each of them on the maxima of their Hilbert envelopes. The resulting reflected and transmitted wave packets are shown in Fig. 8(a) and (b), respectively. The first transmitted pulse [black line on Fig. 8(b)] is roughly out of phase with the subsequent transmitted waves, while the reflected signals are all in phase.

Fig. 9 presents the same type of data as Fig. 7 for a crack tilted at 50° with an effective depth of 75% of the wall thickness with an input five-cycle toneburst at a center frequency $f = 100.0$ kHz. Destructive interference between transmitted wave packets leads to a transmission null at the center frequency, though some transmission is seen due to the significant bandwidth of the input signal. The screenshots of the motion shown in Fig. 10 show that most of the incident signal is reflected; as the crack is shorter than that of Fig. 6, the successive transmitted and reflected wave packets overlap. It is interesting to note that the motion above the crack and the motion below the crack have opposite directions at $t = 330$ μs. This leads to destructive interference in the transmitted signals, so giving the very small transmitted motion seen at $t = 337$ μs.

This behavior shows similarities with reflection from rectangular notches [13]. However, in the notch case, there is a reflection, rather than transmission, minimum. In the notch case, the defect can be modeled as a simple step-down followed by a step-up, leading to the two planes of reflection shown in Fig. 11(a). The first reflected signal, coming from the step-down, is out of phase with all subsequent reflected signals coming from the thinner section of the plate. Given an appropriate notch length, destructive interference between the different reflected waves leads to reflection nulls. In the tilted crack case, there is no significant reflection from the start of the crack, as shown in Fig. 6 at 344.5 μs. There is, however, a significant reflection from the other end of the crack in Fig. 6 at 365.5 μs; therefore, there is only one significant plane of reflection in the main path of the wave, as shown in Fig. 11(b). There is also transfer of energy into trapped waves in the pocket formed by the tilted crack and these waves reverberate. Fig. 7(e) displays the time trace and Fig. 7(f) shows the spectrum of the predicted signal at the root of the tilted crack for the same case as in Fig. 7(a)–(d); this indicates a resonance phenomenon with the amplitude of the trapped waves peaking at the frequency of the transmission null located at $f = 128.7$, 142.1, and 154.5 kHz in Fig. 7(d). The higher amplitude in both the time and frequency domains can be explained by the fact that the effective thickness of the plate is smaller at the location where the trapped wave is recorded, leading to an increase in amplitude. This is analogous to the addition of a resonator to the waveguide, similar to the addition of a Helmholtz resonator to a duct carrying acoustic energy [32], [33], which effectively also has a single plane of reflection, shown in Fig. 11(c). This produces a transmission null at the resonance frequency of the resonator and the width of the transmission minimum increases with the size of the resonator [33], [34]. This explains why the width of the minima in Fig. 4(b) increases with increasing crack depth.

Fig. 12(a) and (b) shows, respectively, the reflection and transmission coefficients of the SH_0 wave mode as a function of the axial extent of a 50% deep tilted crack and the frequency-thickness product. They were computed using the frequency content of the reflected and transmitted signals, similar to Fig. 7(b) and (d), for various tilt values. The axial extent of the crack was then computed based on the frequency at which the reflectivity and transmissibility were taken. There is a clear separation between the measured coefficients below and above the SH_1 cutoff frequency, at around 1.62 MHz·mm. The unity reflections and transmission nulls that can be observed below the SH_1 cutoff frequency are not present once mode

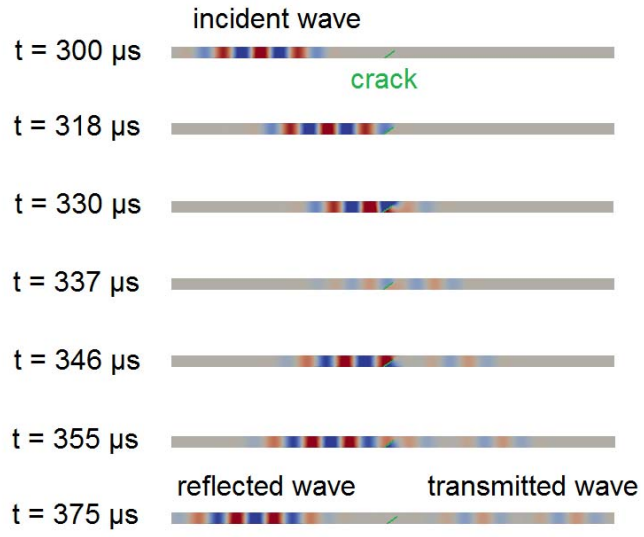

Fig. 10. Screenshots of the amplitude of the horizontal (x-direction in Fig. 1) displacement as an incident SH_0 wave with an input five-cycle toneburst at a central frequency $f = 100.0$ kHz interacts with a 75% depth crack (in green) with a tilt angle of 50° in a 10-mm plate (not to scale).

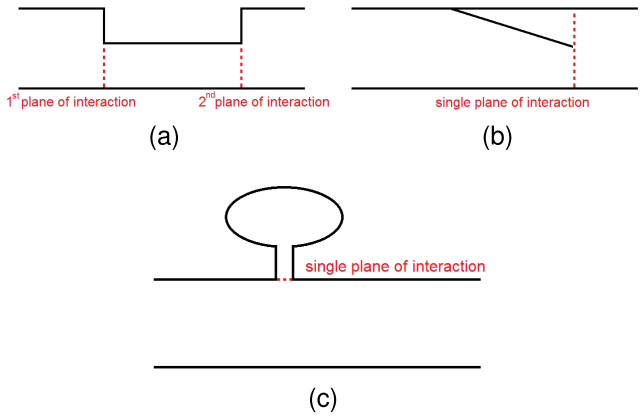

Fig. 11. Planes of interaction for (a) vertical notch, (b) tilted crack, and (c) Helmholtz resonator.

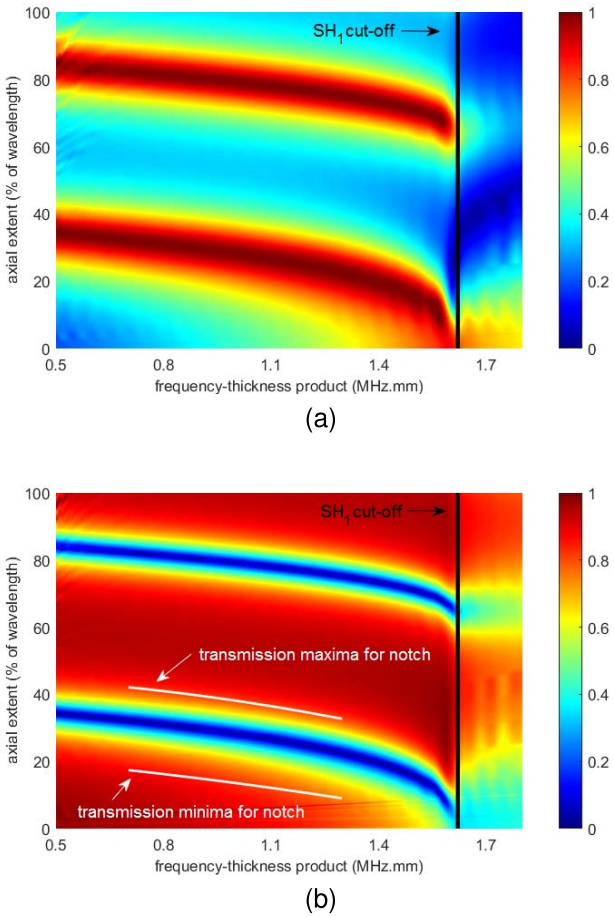

Fig. 12. Coefficients of (a) reflection and (b) transmission as a function of the axial extent of a 50% deep crack and the frequency-thickness product.

conversion to the SH_1 mode can occur. Obviously, the sum of the squares of the SH_0 reflection and transmission coefficients is no longer equal to unity above this limit, as a significant fraction of the incoming SH_0 mode energy is converted to SH_1. Fig. 12 shows a gradual change of the frequency of the extrema in reflection and transmission as the axial extent, and hence the tilt in the case of a tilted crack, varies. The loci of transmission maxima and minima for the notch case are also shown in Fig. 12(b) and also show a gradual change with frequency-thickness product. Demma *et al.* [13] attributed this drift to the frequency dependence of the phase change observed at the step-up and step-down interfaces. It is believed that a similar phenomenon is the driving factor for the variation of the location of the transmission null in the tilted crack case.

IV. Experimental Validation

Two predictions made by the model, the reflectivity of a tilted notch and the presence of a transmission null in certain circumstances, have been validated experimentally. This required the production of two types of specimen; the first comprised a 1000-mm-long, 400-mm-wide, 10-mm-thick steel plate that had a full-width electrical discharge machining (EDM) notch machined 500 mm from one end. Unfortunately, it was not possible to produce the EDM notch at an appropriate angle and depth to generate a transmission null. Therefore, the second type of specimen, 600 mm long, 200 mm wide, and 10 mm thick, was produced using a 2-mm diameter milling cutter; this specimen was made of aluminum, with Poisson's ratio of 0.33, a density of 2700 $kg \cdot m^{-3}$, and Young's modulus of 69 GPa, in order to reduce the probability of tool breakage during manufacture. The angle, depth, and width of the defects are shown in Table II along with the dimensions of the plates. Since the experiments were designed to validate the finite element modeling, the measurements were compared with finite-element predictions using the dimensions and material properties of each specimen, rather than simply with the results for zero width notches presented earlier. The transducers used for these experiments were periodic permanent magnet electromagnetic acoustic transducers (EMATs) [35] with an arrangement of four magnets of alternating polarity at a spacing of 20 mm so the excitation was over a length of 80 mm which is roughly 2.5 wavelengths of the SH0 mode at 100 kHz.

TABLE II
PARAMETERS DESCRIBING THE PLATES USED FOR EXPERIMENTS

Plate number	1	2
Plate		
Metal	steel	aluminium
Length (mm)	1000	400
Width (mm)	600	200
Thickness (mm)	10.0	10.0
Defect		
Depth (mm)	3.3	6.0
Tilt (deg)	40	64
Defect width (mm)	0.35	2.0

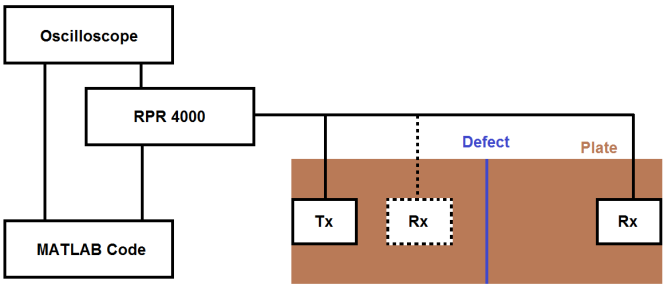

Fig. 13. Setup used for transmission experiments (receiver solid lines) and reflection measurements (receiver: dotted lines).

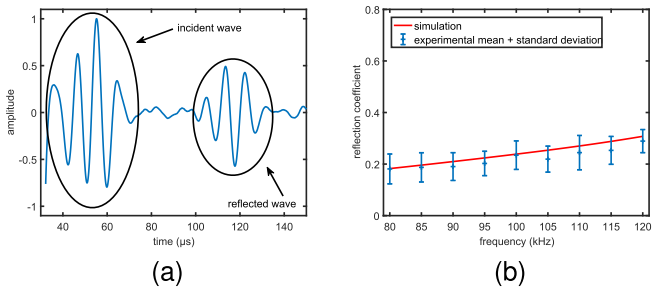

Fig. 14. Experiment on a 350-μm-wide notch in steel plate, with depth = 3.3 mm and tilt = 40° showing (a) example of a time trace recorded by the receiver at 100 kHz and (b) eflection coefficient between 80 and 120 kHz taken every 5 kHz.

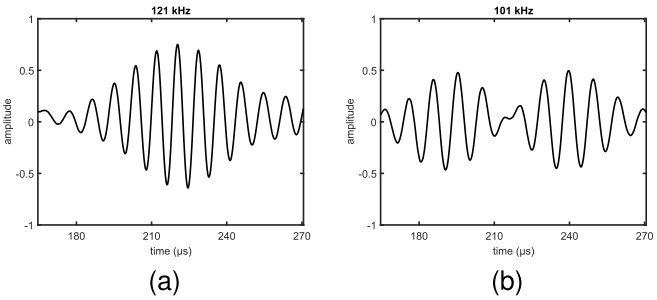

Fig. 15. Normalized time traces of the transmitted waves in the case of a 2-mm-wide notch in aluminum plate, with depth = 6 mm and tilt = 64° for an excitation signal with seven cycles and a center frequency of (a) $f = 121$ kHz and (b) $f = 101$ kHz.

The experimental setup for transmission experiments is shown in Fig. 13, a RITEC pulser–eeceiver (RPR) 4000 being used to generate a seven cycle Hanning-windowed sine wave at a center frequency of 100 kHz, this value being varied in different experiments between 80 and 120 kHz; seven cycles were used to generate a signal with a relatively small bandwidth of 30 kHz at −3 dB. The bandpass filter implemented inside the RPR 4000 was used to remove frequencies outside the range of interest 50–200 kHz. The pulser–receiver was linked to both the EMAT transducers used for signal generation and reception and to a LeCroy waveRunner 44Xi oscilloscope that recorded the received signal. Instruments were configured and data were analyzed using MATLAB. In the case of reflection experiments, both transducers were located on the same side of the defect.

For plate number 1, both transducers were placed on the same side of the defect, the transmitter and the receiver being, respectively, located 250 and 100 mm away from the defect, a typical received signal being shown in Fig. 14(a). The distortion that can be observed at the very beginning of the signal is caused by the end of the ringdown of the amplifier. The reflection coefficient was obtained from the ratio of the signal envelopes of the reflected and incident signals and the experiment was repeated with different center frequencies in 5-kHz steps. Fig. 14(b) shows the predicted and measured reflection coefficients, the uncertainty bars on the measured results showing the standard deviation of eleven measurements. The experimental results agree reasonably well with the predictions; the variation with frequency is modest so using simple envelope amplitudes at different center frequencies to estimate the reflection coefficient is a reasonable approximation. Tests indicated that attenuation due to beam spread and material losses was small compared to the scatter in the experimental results so simply taking the ratio of the amplitudes of the two signals in Fig. 14(a) was satisfactory. The mean reflection coefficient is lower than the predicted values; this is believed to be partly a result of transducer misalignment with the defect since the maximum value would be obtained when the transducers are perfectly aligned normal to the defect. The transducers were fabricated in-house and the elements were not precisely aligned to the casing.

In the case of plate number 2, each transducer was placed at opposite ends of plate, 300 mm away from the defect. The frequency was swept in steps of 1 kHz until a transmission minimum was seen at the center frequency which occurred at a frequency of $f = 101$ kHz. For comparison, another result is shown at a center frequency of $f = 121$ kHz, remote from a transmission minimum. Fig. 15(a) shows the first transmitted pulse at a center frequency of $f = 121$ kHz, the transmitted signal being longer than the incident signal because of the reverberation of the incident wave below the crack. In contrast, Fig. 15(b) shows the result at $f = 101$ kHz where considerable distortion and a lower peak amplitude is evident, similar to the transmitted signal shown in Fig. 9(b) in the case of a simulated transmission null. The incident wave was also measured by moving the receiver to the same side of the defect as the transmitter, 150 mm away from both the transmitter and the defect. Each signal was normalized to the

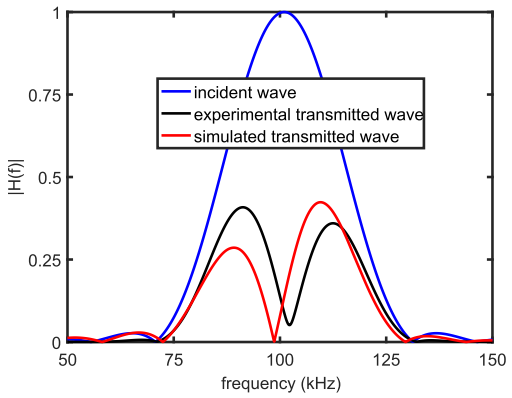

Fig. 16. Frequency spectra of the incident and transmitted waves in the case of a 2-mm-wide notch in aluminum plate, with depth = 6 mm and tilt = 64° between 50 and 150 kHz for an excitation signal with seven cycles and a center frequency $f = 101$ kHz.

measured incident wave, as it has been shown for plate 1 that the short propagation distance does not significantly affect the amplitude of the signal. For each measurement, the transducers were slightly rotated to find the orientation leading to the maximum amplitude of the recorded signal.

Fig. 16 shows the frequency content of both the incident wave and the transmitted signal in the case where a transmission minimum was obtained. The latter is also compared with the spectrum of the transmitted signal obtained from a simulation run at the same center frequency of $f = 101$ kHz. The measurements show a clear transmission minimum at 102 kHz which is in reasonable agreement with the predicted transmission null at 98.6 kHz. The discrepancy comes from the uncertainty on the measurement of the depth, tilt, and width of the defect, leading to the simulation model not being 100% accurate in representing the experimental setup. The minimum observed transmission coefficient is 0.05 rather than the predicted null; here again, it is believed that this may be due to some non uniformity of the notch or transducer misalignment, leading to the transmission minimum not exactly reaching zero.

V. Conclusion

The interaction of the SH_0 wave mode with tilted, surface-breaking cracks in plates at frequency-thickness product values below the SH_1 cutoff frequency has been investigated. Reflection and transmission coefficients from the cracks of different depths and tilt angles were obtained using a finite-element model, with the key results being validated experimentally.

As would be expected from reciprocity, it was found that the direction of the tilt of the crack relative to the incident wave direction does not affect the reflection and transmission behavior; at tilt angles below about 20°, the response is similar to that from a crack normal to the surface. As in the case of a rectangular notch, it was shown that the reflection and transmission coefficients are a function of the axial extent of the crack expressed as a fraction of the wavelength. However, unlike the notch case, a transmission null, and corresponding total reflection, is seen at particular axial extents. The null is present at all the depths studied, but the dip in the transmission versus axial extent curve becomes sharper as the depth of the crack decreases. It was shown that this behavior is analogous to that of acoustic flow in a duct to which a Helmholtz resonator is added; this produces a transmission null whose bandwidth increases with the size of the resonator. It was found that the transmission null disappears at frequencies above the SH_1 cutoff as mode conversion makes the waves reverberating in the crack region more complex.

Experiments were conducted to validate the results obtained using simulation, showing reasonably good agreement with the results from the predictions. The key result of this paper, the transmission null, was observed in the case of a highly tilted notch and the measured value for the location of the transmission null agreed well with the predictions.

The results suggest that testing below the SH_1 cutoff using a broadband input and exploiting the transmission null will enable the detection of shallow cracks that would normally require higher frequency inspection. The relatively simple signals at low frequencies where there is only one propagating SH mode make signal processing much simpler, and it may be possible to use the frequency at which the transmission null occurs to estimate the axial length of the crack. The depth could then be estimated from the sharpness of the transmission minimum. This will be valuable in pigging operations, particularly in high pH environments where tilted cracks tend to occur. Multiple kilometers of pipe need to be covered per day so simple signals and hence simple signal processing would provide major benefits.

Acknowledgment

The authors would like to thank Prof. M. Lowe from Imperial College London, London, U.K., for helpful discussions about the origin of the transmission null.

References

[1] T. Callan, "Pipeline technology today and tomorrow," *OIL GAS Eur. Mag.*, vol. 124, no. 9, pp. 110–115, Mar. 2008.
[2] P. Raczyński and K. Warnke, "Ultrasonic diagnostics of main pipelines," *Adv. Mater. Sci.*, vol. 17, no. 4, Jan. 2017.
[3] V. Varma, R. Tucker, S. Kercel, J. Rose, and W. Luo, "Pipeline flaw detection using shear emat and wavelet analysis," Oak Ridge Nat. Lab., Roane County, TN, USA, Tech. Rep., 2004.
[4] R. Sutherby and W. Chen, "Deflected stress corrosion cracks in the pipeline steel," in *Proc. Int. Pipeline Conf.*, vols. 1–3, 2004, pp. 113–121.
[5] J. Xie, L. Yang, M. Sen, R. Worthingham, and F. King, "Mechanistic investigation of deflected stress corrosion cracking in pipeline steels," in *Proc. NACE Int. CORROSION*, Atlanta, GA, USA, Mar. 2009, pp. 22–26.
[6] L. Zadow, E. Gamboa, and O. Lavigne, "Inclined stress corrosion cracks in gas pipeline steels: Morphology and implications," *Mater. Corrosion*, vol. 66, no. 10, pp. 1092–1100, Oct. 2014.
[7] O. Lavigne, E. Gamboa, V. Luzin, and M. Law, "Analysis of intergranular stress corrosion crack paths in gas pipeline steels; straight or inclined?" *Eng. Failure Anal.*, vol. 85, pp. 26–35, Mar. 2018.
[8] E. Gamboa, M. Giuliani, and O. Lavigne, "X-ray microtomography observation of subsurface stress corrosion crack interactions in a pipeline low carbon steel," *Scripta Mater.*, vol. 81, pp. 1–3, Jun. 2014.
[9] R. Guan, Y. Lu, W. Duan, and X. Wang, "Guided waves for damage identification in pipeline structures: A review," *Struct. Control Health Monitor.*, vol. 24, no. 11, p. e2007, Mar. 2017.
[10] D. N. Alleyne and P. Cawley, "The interaction of Lamb waves with defects," *IEEE Trans. Ultrason., Ferroelectr., Freq. Control*, vol. 39, no. 3, pp. 381–397, May 1992.

[11] R. Chennamsetti, "Interaction between the fundamental Lamb modes and the front edge of a crack in a metallic plate," *IEEE Trans. Ultrason., Ferroelectr., Freq. Control*, vol. 60, no. 6, pp. 1152–1164, Jun. 2013.
[12] C. Schaal and A. Mal, "Lamb wave propagation in a plate with step discontinuities," *Wave Motion*, vol. 66, pp. 177–189, Nov. 2016.
[13] A. Demma, P. Cawley, and M. Lowe, "Scattering of the fundamental shear horizontal mode from steps and notches in plates," *J. Acoust. Soc. Amer.*, vol. 113, no. 4, pp. 1880–1891, Apr. 2003.
[14] R. Carandente, J. Ma, and P. Cawley, "The scattering of the fundamental torsional mode from axi-symmetric defects with varying depth profile in pipes," *J. Acoust. Soc. Amer.*, vol. 127, no. 6, pp. 3440–3448, Jun. 2010.
[15] J. Lee, J. D. Achenbach, and Y. Cho, "Use of the reciprocity theorem for a closed form solution of scattering of the lowest axially symmetric torsional wave mode by a defect in a pipe," *Ultrasonics*, vol. 84, pp. 45–52, Mar. 2018.
[16] M. Koshiba, K. Hasegawa, and M. Suzuki, "Finite-element solution of horizontally polarized shear wave scattering in an elastic plate," *IEEE Trans. Ultrason., Ferroelectr., Freq. Control*, vol. UFFC-34, no. 4, pp. 461–466, Jul. 1987.
[17] J. J. Ditri, "Some results on the scattering of guided elastic SH waves from material and geometric waveguide discontinuities," *J. Acoust. Soc. Amer.*, vol. 100, no. 5, pp. 3078–3087, Nov. 1996.
[18] A. Pau, D. V. Achillopoulou, and F. Vestroni, "Scattering of guided shear waves in plates with discontinuities," *NDT & E Int.*, vol. 84, pp. 67–75, Dec. 2016.
[19] C. Linton, M. McIver, P. McIver, K. Ratcliffe, and J. Zhang, "Trapped modes for off-centre structures in guides," *Wave Motion*, vol. 36, no. 1, pp. 67–85, Jun. 2002.
[20] R. Porter, "Trapped waves in thin elastic plates," *Wave Motion*, vol. 45, nos. 1–2, pp. 3–15, Nov. 2007.
[21] E. Glushkov, N. Glushkova, A. Eremin, and V. Giurgiutiu, "Low-cost simulation of guided wave propagation in notched plate-like structures," *J. Sound Vib.*, vol. 352, pp. 80–91, Sep. 2015.
[22] E. Glushkov, N. Glushkova, M. V. Golub, J. Moll, and C.-P. Fritzen, "Wave energy trapping and localization in a plate with a delamination," *Smart Mater. Struct.*, vol. 21, no. 12, p. 125001, Oct. 2012.
[23] E. Glushkov, N. Glushkova, A. Eremin, and R. Lammering, "Trapped mode effects in notched plate-like structures," *J. Sound Vib.*, vol. 358, pp. 142–151, Dec. 2015.
[24] E. Glushkov, N. Glushkova, A. Eremin, and R. Lammering, "Trapped modes and resonance wave transmission in a plate with a system of notches," *J. Sound Vib.*, vol. 412, pp. 360–371, Jan. 2018.
[25] E. Glushkov, N. Glushkova, M. Golub, and A. Boström, "Natural resonance frequencies, wave blocking, and energy localization in an elastic half-space and waveguide with a crack," *J. Acoust. Soc. Amer.*, vol. 119, no. 6, pp. 3589–3598, Jun. 2006.
[26] S. I. Rokhlin, "Resonance phenomena of Lamb waves scattering by a finite crack in a solid layer," *J. Acoust. Soc. Amer.*, vol. 69, no. 4, pp. 922–928, Apr. 1981.
[27] F. Feng and S. Lin, "The band gaps of Lamb waves in a ribbed plate: A semi-analytical calculation approach," *J. Sound Vib.*, vol. 333, no. 1, pp. 124–131, Jan. 2014.
[28] P. C. Vinh, T. T. Tuan, D. X. Tung, and N. T. Kieu, "Reflection and transmission of SH waves at a very rough interface and its band gaps," *J. Sound Vib.*, vol. 411, pp. 422–434, Dec. 2017.
[29] L. Börgesson, "ABAQUS," in *Coupled Thermo-Hydro-Mechanical Processes of Fractured Media*, vol. 79. Amsterdam, The Netherlands: Elsevier, 1996, pp. 565–570.
[30] P. Huthwaite, "Accelerated finite element elastodynamic simulations using the GPU," *J. Comput. Phys.*, vol. 257, pp. 687–707, Jan. 2014.
[31] P. Cawley, M. J. S. Lowe, D. N. Alleyne, B. Pavlakovic, and P. D. Wilcox, "Practical long range guided wave inspection–applications to pipes and rail," *Mater. Eval.*, vol. 61, no. 1, pp. 66–74, 2003.
[32] D. V. Bazhenov, L. A. Bazhenova, and A. V. Rimskii-Korsakov, "Noise silencer in the form of a helmholtz resonator at the outlet of an air duct of finite length," *Acoust. Phys.*, vol. 46, no. 3, pp. 256–260, May 2000.
[33] L. Bjørnø, "Acoustics: An introduction to its physical principles and applications," *Ultrasonics*, vol. 21, no. 3, pp. 141–142, May 1983.
[34] L. E. Kinsler, A. R. Frey, and A. B. Coppens, *Fundamentals of Acoustics*. Wood Dale, IL, USA: Paperbackshop UK Import, 1999. [Online]. Available: https://www.ebook.de/de/product/4286916/lawrence_e_kinsler_austin_r_frey_alan_b_coppens_fundamentals_of_acoustics.html
[35] R. Thompson, "Physical principles of measurements with EMAT transducers," in *Ultrasonic Measurement Methods*. Amsterdam, The Netherlands: Elsevier, 1990, pp. 157–200.

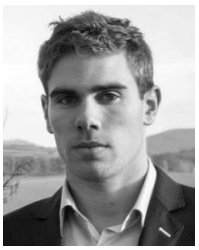

Jérôme Combaniere was born in Toulouse, France, in 1991. He received the M.Sc. degree in electronics and signal processing from the Ecole Nationale Supérieure d'Electrotechnique, d'Electronique, d'Informatique, d'Hydraulique et des Télécommunications, Toulouse, France, in 2016. He is currently pursuing the D.Eng. degree with the Non-Destructive Testing Group, Imperial College London, London, U.K.

He developed an interest in the field of guided waves during his internship in Germany, as part of his cursus to graduate, where he worked on automating data acquisition and assessment for a tool based on various guided wave types. He is currently with BHGE, a GE Company, where he is working on the interaction between guided waves and complex defects.

Peter Cawley was born in Sheffield, England, U.K., in 1953. He received the B.Sc. and Ph.D. degrees in mechanical engineering from the University of Bristol, Bristol, U.K., in 1975 and 1979, respectively.

He worked in industry from 1979 to 1981 and then joined the Mechanical Engineering Department, Imperial College, London, U.K., initially as a Lecturer and then successively as a Senior Lecturer, a Reader, and a Professor. He has worked on a wide variety of projects using sonic and ultrasonic methods applied to the Non-Destructive Evaluation (NDE) and he leads the NDE Group, Imperial College London. He is currently the Head of the Mechanical Engineering Department. He is also a Director of two spin-out companies set up to exploit technology developed in his research group (Guided Ultrasonics Ltd., Brentford, U.K., and Permasense Ltd., Crawley, U.K.), and also a consultant to a variety of industries. He is also a leading member of the U.K. Research Centre for NDE that has its head office at Imperial College London. He has authored or coauthored more than 160 refereed journal papers and a similar number of conference papers in this field and holds four current patents.

Kevin McAughey received the B.Sc. degree in physics from The University of Warwick, Coventry, U.K., in 2009, the M.Sc. degree by Research in high temperature piezoelectric films in 2011, and the Ph.D. degree in non-destructive evaluation in 2015, focusing on guided wave ultrasonics generated and detected by electromagnetic acoustic transducers. He joined GE in 2014, where he continued to work EMATs and guided waves, while also gaining experience in other disciplines, including phased array ultrasonics and magnetic flux leakage. He has a wide variety of technical responsibilities, from transducer design and manufacture, and to data analysis and interpretation. Since 2016, he has supervised two D.Eng. students, with a third starting in 2018.

Jochen Giese received the Dipl.Ing. and D.E.A. degrees from the University of Karlsruhe, Karlsruhe, Germany, and the Institut National Polytechnique de Grenoble, Grenoble, France, respectively, in 1999, and the Ph.D. degree from the Royal Institute of Technology, Stockholm, Sweden, in 2005. He joined Qualcomm CDMA Technologies GmbH, Nuremberg, Germany, in 2006, and contributed to the development of third and fourth generation mobile communication systems before changing his professional interests to non-destructive testing in 2011. Since 2011, he has been leading research and development teams to advance in-line pipeline inspection devices based on several sensing technologies, including piezo-ceramic and electromagnetic acoustic transducers. His main research interests are in ultrasound modeling and imaging, general signal and data processing, and algorithm design.